PCCP

Accepted Manuscript

ROYAL SOCIETY OF CHEMISTRY

www.rsc.org/pccp

Journal Name

ARTICLE

O_2 and H_2O_2 Transformation Steps for Oxygen Reduction Reaction Catalyzed by Graphitic Nitrogen-doped Carbon Nanotubes in Acidic Electrolyte from First Principles Calculations

Received 00th January 20xx,
Accepted 00th January 20xx

DOI: 10.1039/x0xx00000x

www.rsc.org/

Yuhang Li, Guoyu Zhong, Hao Yu, Hongjuan Wang and Feng Peng*

It is highly challenging but extremely desirable to develop carbon catalysts with high oxygen reduction reaction (ORR) activity and stability in acidic medium for commercial application. In this paper, based on density functional theory (DFT) calculations with long rrange interaction correction and solvation effect, the elementary transformations of all the probable intermediates in ORR and hydrogen peroxide reduction reaction (HPRR) over graphitic nitrogen-doped carbon nanotubes (NCNTs) in acidic medium were evaluated, finding that all the rate determining steps are related to the bonding hydroxyl because of the strong interaction between hydroxyl and carbon. Thus, the direct four-electron ORR and the two-electron HPRR are hard to proceed. Together with hydrogen peroxide disproportionation (HPD), a mixed mechanism for ORR in acidic electrolyte was proposed, where the two-electron, three-electron ORRs and HPD dominate the electrode reaction. The experimental result for ORR catalyzed by NCNTs in acidic electrolyte also well illustrated the rationality of theoretical calculations. This study not only gives new insights into the effect of graphitic nitrogen doping on ORR catalyzed by carbon, but provides a guide to design carbon catalysts with high ORR activity in acidic electrolyte.

Introduction

Leaning on utilization of clean and efficient energy sources, human society is stepping forward in a sustainable way. Fuel cells, one of renewable energy conversion and storage technologies, play a vital role to achieve this goal. However, the drawbacks of platinum group metal (PGM) catalysts for oxygen reduction reaction (ORR) at the cathode restrict the extensive application of this technology, such as rare reserve, high cost and poisoning effect[1, 2]. Aiming at the search of substitute catalysts, carbon-based nanomaterials have attracted interests of many researchers. Especially, nitrogen-doped carbon nanotubes (NCNTs) and correlative materials show a nice performance in alkaline electrolyte for ORR due to the activation of carbon by nitrogen atoms, which has been confirmed both by experiments[3-5] and theoretical calculations[6]. Nevertheless, their activity remains inferior to PGM in acidic electrolyte[7, 8] and it is still debatable about active sites and the authentic mechanism[9-11]. However, current polymer electrolyte membrane fuel cells work in an acidic environment because Nafion is widely used as the proton-transfer electrolyte[12]. Thus, it is highly challenging but extremely desirable to develop carbon catalysts with high ORR activity and stability in acidic medium for commercial application.

As a novel metal-free catalyst, some electronic properties of NCNTs are different from those of metallic materials. The complex orbital hybridization of metal, to some extent, makes it more flexible for the adsorption and the desorption of small molecules[13, 14]. On the other hand, the high electron delocalization in metal is beneficial for the electron migration inside materials and the electron transfer between the metal and intermediates, which can be related to the chemical bonding dynamics. The nitrogen doping can modify the original electronic structure of pure CNTs and reduce the conductivity[15-17], but NCNTs still remain the high electron delocalization and perform a nice activity in ORR. From previous experimental investigations, the apparent electron transfer number of ORR catalyzed by NCNTs in acidic medium ranges from two to three[18, 19], meaning that the two-electron reduction of oxygen dominates the electrode reaction. Because the main product for two-electron ORR is hydrogen peroxide[20] and it is unstable over the surface of NCNTs, the overall reaction should contain oxygen reduction and hydrogen peroxide reduction reaction (HPRR). To this end, it is of particular worth to figure out the elementary transformation dynamics of all the probable intermediates in ORR and HPRR so as to seek out limiting steps and shift ORR to the direct four-electron process.

In this contribution, we divided the overall oxygen reduction process into four reactions: direct four-electron oxygen reduction, two-electron oxygen reduction, two-electron hydrogen peroxide reduction and the disproportionation of hydrogen peroxide. Through the

School of Chemistry and Chemical Engineering, South China University of Technology, Guangzhou, 510640, China. Email: cefpeng@scut.edu.cn; Tel/Fax: +86-20-87114916

† Electronic Supplementary Information (ESI) available. See DOI: 10.1039/x0xx00000x

electronic structure and the energy calculations, we proposed a reliable mixed mechanism to understand the overall reaction. This study not only gives new insights into the effect of graphitic nitrogen doping on ORR catalyzed by carbon, but provides a guide to design carbon catalysts with high ORR activity in acidic electrolyte.

Computational methods

Density functional theory (DFT) calculations were performed with the DMol3 package[21] in Materials Studio. Exchange-correlation functions were described by generalized gradient approximation (GGA) with Perdew-Burke-Emzerhof (PBE)[22]. All electron method was adopted as the core treatment. Double numerical plus polarization (DNP) was employed as the basis set and the orbital cutoff of 4.5 Å was assigned to global atoms. To make the calculations accurate and reliable, Grimme[23] method was pondered for the long range interaction correction. The convergence tolerance of self-consistent field (SCF) calculations was 1.0×10^{-6} Ha. For the task of geometry optimizations, the convergence in energy and the maximal force were 1.0×10^{-5} Ha and 2.0×10^{-3} Ha/Å, respectively. The k-point of the first Brillouin zone (FBZ) was set to 1×1×24, which was same for density of states (DOS) calculations. In order to characterize the polarization effect of water solution, the conductor-like screening model (COSMO)[24, 25] with the permittivity of 78.54 was employed throughout our work. In the tasks about transition state (TS), linear synchronous transit (LST)[26] with quadratic synchronous transit (QST) method was used to search TS and nudged elastic band (NEB)[27] method was used to confirm TS.

We considered a (5,5) carbon nanotube, which was extended to a (1×1×4) supercell, in the three-dimensional period lattice with the parameters (Å) of 25×25×9.838. In our previous experimental analysis of XPS, the primary and secondary nitrogen species were graphitic and pyridinic, respectively (Fig. S1). These two nitrogen species are supposed as the active sites for ORR. We focused on the graphitic doping because we compared the oxygen adsorption process and found that the pyridinic nitrogen is inferior to the graphitic nitrogen (Fig. S2). According to the investigation of several nitrogen doping configurations by Chai et al.[6], the unit with two graphitic nitrogen atoms at the para-position was one of activated configurations, so we replaced C atoms with two N atoms at the para-position of the hexagonal ring, standing for the doping concentration of 2.5%. For the sake of π-bonding system, we used the Hirshfeld[28] population analysis method to describe the charge distribution in NCNTs. The more details of parameter settings in calculation and analysis were provided in following paragraphs or Supporting Information.

Results and discussion

Reaction paths design

For the overall oxygen reduction process in acidic electrolyte, there are two situations to be considered. One is that O_2 will be reduced directly to H_2O via a four-electron path and the other is that O_2 will be reduced to H_2O_2 first via a two-electron path, then H_2O_2 to H_2O. All probable steps for both O_2 and H_2O_2 reductions are designed into reaction networks, as shown in Fig. 1. It is noteworthy that the intermediates called the same name may refer to different configurations because the atom or molecule can adsorb at different sites. In order to distinguish them, all the intermediates in this paper are marked as a format of "element" with "number", where the number points to adsorption sites, corresponding to Fig. 2.

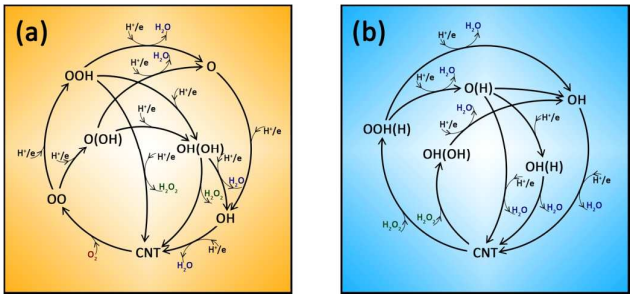

Fig. 1 The designed overall reaction networks of (a) O_2 and (b) H_2O_2 reductions. All the atoms or molecules are adsorbed at active sites in NCNTs. The part in parenthesis represents the co-adsorption together with that outside parenthesis.

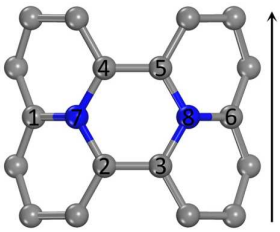

Fig. 2 The partial structure of graphitic nitrogen-doped CNTs. The arrow stands for the axial direction of nanotubes. The gray ball is carbon and the blue ball is nitrogen. Bond lengths (Å) of 1-7, 2-7 and 2-3 are 1.402, 1.418 and 1.398, respectively.

In the oxygen reduction process (Fig. 1a), the first step is O_2 adsorption, which results in two product configurations including ring (OO23) adsorption and chain (OO1) adsorption.

For the first electron step:

$$OO + e^- + H^+ \rightarrow OOH \text{ or } O(OH) \quad (1)$$

The system is injected with one electron and combine with a hydrion close to catalyst surface, to generate OOH or O(OH) according to the breaking of O-O bond or not.

For the second electron step:

$$OOH + e^- + H^+ \rightarrow O + H_2O \text{ or } OH(OH) \text{ or } H_2O_2 \quad (2)$$

$$O(OH) + e^- + H^+ \rightarrow O + H_2O \text{ or } OH(OH) \quad (3)$$

$$OH(OH) \rightarrow H_2O_2 \quad (4)$$

When the OOH configuration formed, both oxygen atoms are activated so that there is H_2O_2 produced if the hydrion attacks the oxygen bonding to NCNTs. Otherwise, if the

hydrion acts on another oxygen atom, one H_2O molecule is produced and leave a lone oxygen atom bonding to carbon. When O(OH) is formed and one hydrion gets close to the lone oxygen, it may be transformed into a configuration where two hydroxyls are bonding to the nanotube. In details, there are two bonding types for hydroxyls named OH(OH)23 and OH(OH)35, which leads to different variations in the following energy analysis. If in a more special case, the desorption happens at the same time for two hydroxyls to generate one H_2O_2 molecule.

For the third electron step:

$$O + e^- + H^+ \rightarrow OH \quad (5)$$

$$OH(OH) + e^- + H^+ \rightarrow OH + H_2O \quad (6)$$

Whether the lone oxygen or two hydroxyls structures, they are all transformed to the OH intermediate when the system obtains one electron and combines with one hydrion.

For the fourth electron step:

$$OH + e^- + H^+ \rightarrow H_2O \quad (7)$$

There is almost only one way turning OH to H_2O and the NCNTs catalyst gets back to the original status.

However, the reduction step analyses of H_2O_2 are similar to those of O_2 and the main difference between them lies in the H_2O_2 adsorption step. When a H_2O_2 molecule diffuses to active sites, the O-O bond may be broken and two generated hydroxyls link to nanotubes (called cracked adsorption). For another possibility, H_2O_2 first ionizes into OOH^- and H^+ then the ions adsorb on nanotubes (called ionized adsorption). The product OH(OH) or OOH(H) participates in next reduction steps, which are analogous to the reactions of oxygen.

The migration of hydronium

In aqueous solution, the proton is hydrated by several water molecules through the strong electrostatic interaction, forming $H^+(H_2O)_n$ configuration series[29, 30]. And for the elimination of errors which are brought by the DFT calculation on a particle without electron, the simplest hydrated proton H_3O^+ (hydronium) was used realistically throughout our work. To study the migration process of hydronium from the solution bulk phase to active sites on the nanotube surface, we focused on energy and charge properties of the system consisting of NCNTs and one hydronium cluster. The cell height parameter was enlarged to 50 Å for more space to move hydronium and the calculation results are shown in Fig. S3. In order to explore the impact of active sites (AS) on migration, the case of inactive sites (IS) is set as contrast. The hydronium, with an initial distance of 15 Å, approaches nanotube surface gradually along with the total system energy declining until about 5 Å. According to the electrical double layer theory and the COSMO invisible solvation modelling, the charged electrode attracts particles with the opposite charge or polarizes the solvent molecules, which is expressed as screening charge on COSMO surface around nanotubes. So the opposite potential field in the double layer (Also described by the region outside the COSMO cavity) hinders the approach of hydronium. However, the repulsion for hydronium is quite weak when the distance is greater than 5 Å and the electrostatic attractant interaction plays a dominant part, leading to the decline of system energy for both cases of AS and IS. During the movement, hydronium can hold its positive charge at 1.00 e and the nanotube can hold its negative charge at -1.00 e, indicating that there is not any electron transfer in the system. This process may occur in the diffuse layer on the basis of electrical double layer theory. Hydronium continues closing to the nanotube from 5 Å and the total system energy rises rapidly for both cases. In comparison, when a hydronium approaches to AS, the energy goes up more sharply than the other case. This result shows that it is an endergonic process for hydronium passing through the inside of electrical double layer, which is in line with the compact layer. Starting from about 5 Å, the surface of nanotubes assembles numerous opposite ions or polarized molecules, causing the increase of repulsive interaction between hydronium and screening charge. From a previous ab-initio dynamics investigation about the water/graphene system by Michaelides et al.[31], the density of water increases rapidly starting from 4.5 Å to surface, which suggests that the polarized positive charge gets more intensive and the repulsion for hydronium gets stronger. In this process, the positive charge on hydronium starts to decrease, showing that the electron transfer happens. Nevertheless, the mechanism of transfer is not specific especially at the beginning stage of charge decline. We speculate that the change of charge density might be caused by the shift of electron cloud to hydronium because of the electrostatic attraction, and the polarization via the solvent molecules between active sites and hydronium[32].

Due to the complicated solvent potential field around CNTs, we have performed a substitute modeling where a graphene structure with the same doping formation as NCNTs was used to obtain the COSMO field (See Fig. S4). During calculations, the optimized monolayer N-doped graphene was set into the three-dimensional period lattice with the parameters (Å) of 12.422×12.806×50 and other parameters for graphene system calculation entirely kept pace with NCNTs system except that k-point was set to 6×6×1. As shown in the distribution of COSMO field, the screening charge is almost zero above 20 Å and the repulsive interaction is weak enough to be negligible. In diffuse layer, polarization caused by charged graphene strengthens slowly. If narrowed to 5 Å, it starts to enter the high potential region, which is in agreement with the energy analysis above. When hydronium migrates to the position less than 3 Å, chemical reactions will happen such as the proton escape from hydrated clusters and the combination of proton with charged intermediates. The COSMO modelling contributes an authentic solvent environment for calculations about electrode reaction dynamics. In acidic electrolyte, the NCNTs assemble more water molecules in the compact layer than bulk phase and generate a relatively strong positive potential field to hinder the hydronium migration. Hence, the electrode should provide additional energy to neutralize the migration repulsion.

Energy variations in transformation steps of oxygen

The reduction reactions of oxygen and hydrogen peroxide are discussed separately in terms of the designed networks in Fig. 1. All the initial system energies were set to zero. First, the oxygen molecule can stay at a stable configuration under the physisorption with nanotubes due to the system energy declines of about 0.2 eV from the isolated system. The energy barrier for OO23 generating is 0.309 eV, which is greater than 0.113 eV for OO1 generating (See Fig. 3 and Table S1 about the corresponding values, similarly hereinafter). The chain adsorption leads to an activated state, with the endoergic reaction energy variation of 0.105 eV. The ring adsorption is an exoergic process with the energy of -0.341 eV. The O-O bond is elongated in both cases, which means an electron transfer process and an oxygen activation process.

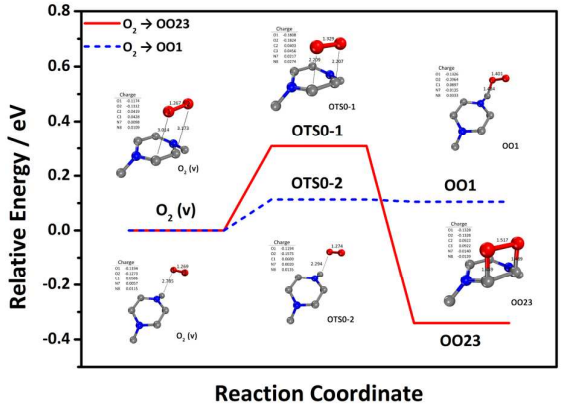

Fig. 3 Energy evolutions for the oxygen molecule adsorption on the different sites. (v) means that the molecule is under a long-range physisorption interaction with the distance of about 3.8 Å. Atomic numbers of carbon and nitrogen refer to Fig. 2.

From the population analysis marked in Fig. 3, when the ring adsorption proceeds, electron cloud is first deviated from nitrogen to oxygen to reach transition state. When the C-O bond is generated, partial negative charge in oxygen is transferred back to nitrogen in order to reduce the system energy and finish adsorption. It is analogous to chain adsorption. The nitrogen away from oxygen first donates electron cloud to the lone oxygen atom. When C and O are under chemisorption, the nitrogen near oxygen will be assembled with a few negative charges to equilibrate the system. So far as that goes, the nitrogen doping in CNTs is a vital electron donor to generate transition states and redistribute charges. The oxygen activation can be analyzed further by partial density of states (PDOS), as shown in Fig. 4d. The active electron density of the oxygen atom in OO23 declines to zero compared with the isolated free oxygen, indicating that OO23 is a stable four-membered ring state instead of activated oxygen state. For OO1, the outside lone oxygen atom is activated because the PDOS at Fermi level increases and more electrons are assembled at high energy level. From the band structure analyses of Figs. 4a-c, the conductivity gets lower slightly after oxygen adsorption but there is no significant changes. The chain adsorption OO1 changes the energy level configuration near Fermi level, which is in line with PDOS analyses.

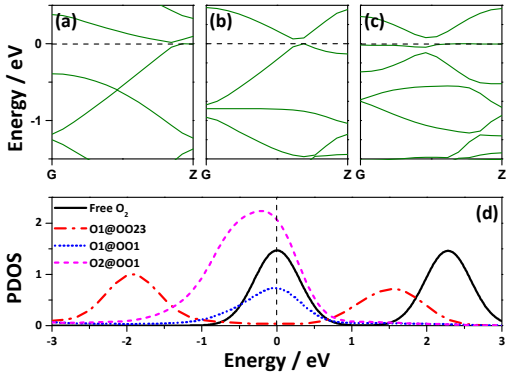

Fig. 4 Band structures of (a) pure NCNT, (b) OO23 and (c) OO1. (d) The partial density of states (PDOS) for different oxygen atoms. Zero energy is set as Fermi level.

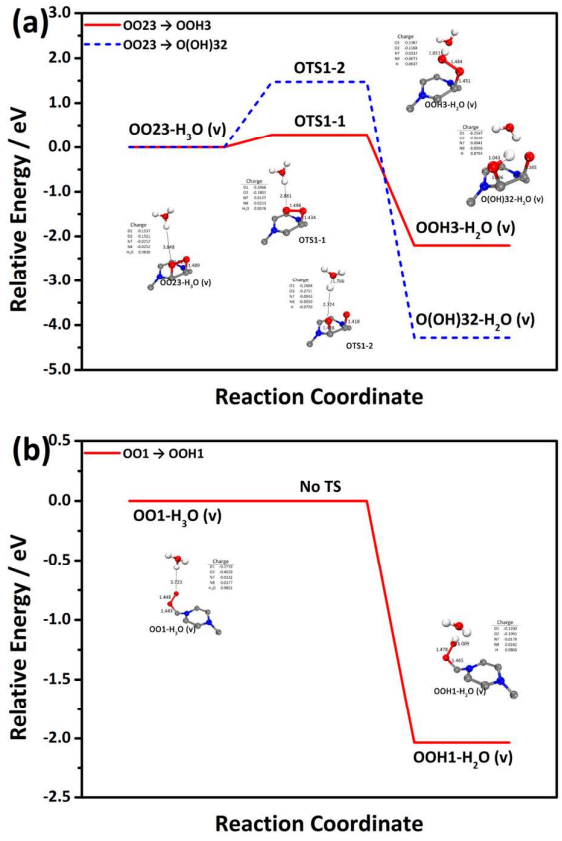

Fig. 5 Energy evolutions for the first electron reaction in ORR from initial systems (a) OO23 and (b) OO1.

For the first electron reaction in ORR, the energy evolutions and intermediate structures are shown in Fig. 5. If the ring adsorption of oxygen happens, it will be almost impossible to break the O-O bond to form O(OH)32 structure because an energy barrier of 1.474 eV exists in this process. In comparison, OOH3 structure is easier to be generated with a

low barrier of 0.286 eV. If the chain adsorption happens, OOH1 structure will be formed without transition state only if hydronium migrates against the repulsion to active sites of NCNTs. From the analysis on structures, one of C-O bonds in the stable four-membered ring must be broken to reach transition state (OTS1-1), along with the electron transfer to oxygen. When the hydronium approaches, the assembled negative charge on oxygen is transferred to hydrogen. The role of nitrogen in the reduction process is enriching and releasing electrons, just like an "interchange". However, if one electron enters OO1 system, the charge of the lone oxygen atom gets more negative and the hydronium is under a strong electrostatic attraction. As a result, along the decline tendency of potential energy, OOH1 is formed rapidly. As shown in Figs. S5b-c, the original highest symmetric point in FBZ has a down shift and turns into the valence band, indicating that the OOH cluster is a strong electron acceptor in the nanotube system and the assembled electrons can be donated to hydronium. Both OOH3 and OOH1 have good conductivities due to the energy level continuity near Fermi level. Compared with OOH3, the active electron in OOH1 occupies a higher level and the charge density is higher (See Fig. S5a), suggesting that the oxygen in OOH1 has more possibility to be reacted. To summarize, O1 atom in OOH1 is the most activated.

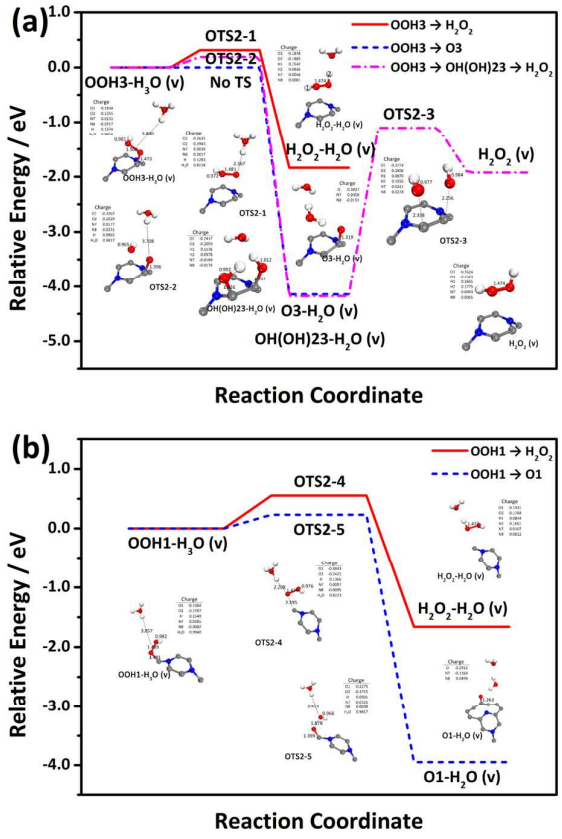

Fig. 6 Energy evolutions for the second electron reaction in ORR from the probable initial systems (a) OOH3 and (b) OOH1.

For the second electron reaction in ORR, the key point locates whether H_2O or H_2O_2 is to be generated. First, the initial reactant OOH3 can bring out four different products and the probable three of them are shown in Fig. 6a. The other impossible case was also calculated and results are shown in Fig. S6a. When hydronium approaches to the inside oxygen atom (Marked O2 in figure), hydrogen peroxide may be generated along with the bond breaking of C-O (OTS2-1). The energy barrier for this process is 0.313 eV. In another case, the O-O bond may be broken to generate OH(OH)23, with the barrier of 0.191 eV. We wondered if OH(OH)23 could desorb easily to form H_2O_2, so we calculated OTS2-3 and found it is an impossible process. It is a stable adsorption configuration that two hydroxyls link to adjacent carbon atoms. If hydronium approaches to the outside oxygen atom (Marked O1 in figure), without energy barrier, the product O3 is generated. The O-O bond in OOH cluster becomes weak when one electron enters the system. Starting from the reactant OOH1 (See Fig. 6b), the energy barriers for generations of H_2O_2 and O1 are 0.553 eV and 0.231 eV, respectively, which are both higher than the reactant OOH3. The nitrogen doping distribution leads to this result. For OOH3, the adsorption site of intermediates is around two nitrogen atoms, while there is only one nitrogen atom near the adsorbed cluster in OOH1 system. As stated in the previous section, the electron interchange effect of nitrogen contributes to reaching transition states and stabilizing products. This effect in OOH1 is weaker than in OOH3, thus more energy is in need to activate intermediates for OOH1. In other words, the reaction possibility is higher and the reaction rate is faster at the site rich in nitrogen. As shown in Fig. S7a, the oxygen atoms in two products are both in the high activity because they occupy the high energy level near Fermi level. In details, the occupied state of the oxygen atom in O3, as a whole, is shifted to the high level and show a more density at the highest occupied level than that in O1. From the analysis of band structures (See Figs. S7b-c), O3 system owns a bigger energy gap than O1 but both are still in a good conductivity. The variation starting from O(OH)32 reactant is shown in Fig. S6b. Because of the difficulty for O(OH)32 generation in the first electron step, we describe it in SI.

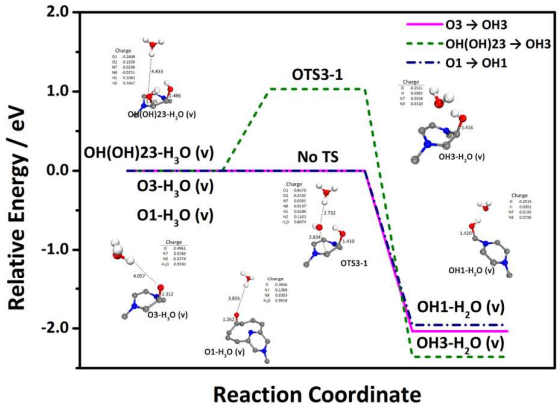

Fig. 7 Energy evolutions for the third electron reaction in ORR from the probable initial systems O3, OH(OH)23 and O1

For the third electron reaction in ORR, starting from O3 or O1 reactant, there are no transition states in the processes due to the negative charge on the lone oxygen atom (Fig. 7). In other words, only if hydronium approaches to the charged oxygen, hydroxyl can be generated easily along with the electron transfer from NCNTs to hydronium. The nitrogen, playing the same role, controls the charge to equilibrate the system in the reaction process. Another noteworthy point for O1 system is that the C-N bond is broken and the carbon atom is almost in an entire sp^2 hybridization state with two adjacent carbon atoms and one oxygen atom. The nitrogen is transformed from graphitic type to pyridinic type. After the generation of hydroxyl, the C-N bond is reformed and the sp^3 hybridization of carbon reappears. Starting from OH(OH)23 reactant, it is difficult to desorb hydroxyl to generate the transition state (OTS3-1) because the C-O bond is quite stable. From the view of charge population, it needs much energy to concentrate negative charge on the hydroxyl, which goes against the electron transfer to hydronium. As shown in Fig. S8a, the highest occupied energy level of O@OH1 is higher than that of O@OH3, indicating that the intensive distribution of nitrogen does not always activate intermediates. At least, it is more activated for the hydroxyl around fewer nitrogen. Band structures of two products are shown in Figs. S8b-c. Hydroxyl acts as a strong electron acceptor in reaction system and both OH3 and OH1 maintain the good conductivity. The unlikely variation starting from OH(OH)35 reactant is analyzed in SI, corresponding to Fig. S9.

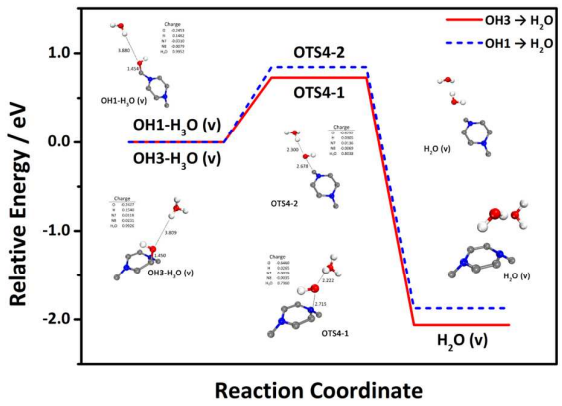

Fig. 8 Energy evolutions for the fourth electron reaction in ORR from the probable initial systems OH3 and OH1

For the fourth electron reaction in ORR, the OH3 reactant needs 0.729 eV and the OH1 reactant needs 0.845 eV to reach transition states (See Fig. 8). Actually, this is the rate determining step if simply considering the reaction dynamic process in acidic electrolyte. The hydroxyl bonding to carbon is stable because of the strong interaction between carbon and oxygen. At this point, the carbon atom is under sp^3 hybridization and the oxygen atom is under saturated sp2 hybridization. So it is difficult to assemble negative charge to hydroxyl and break the C-O bond. In comparison, the reduction starting from OH3 is easier, illustrating that the intensive distribution of nitrogen plays both promotion and inhibition roles at different steps.

Energy variations in transformation steps of hydrogen peroxide

Transformation steps of hydrogen peroxide were also considered because it could be generated easily in the second electron step of ORR, which was verified from the investigation by Girault et al.[33, 34] and our calculations above. We proposed two reaction types, electroreduction and disproportionation. Anyway, the first step is the adsorption process between hydrogen peroxide and NCNTs. There are two probable adsorption ways in acidic electrolyte. First, the O-O bond of hydrogen peroxide may be broken to generate two hydroxyl free radicals, which is named as “cracked adsorption”. Second, one of O-H bonds may be broken to generate H^+ and OOH^-, which is named as “ionized adsorption”. The reason why we consider ionized adsorption is that there is weak ionization for H_2O_2 in the aqueous solution. As shown in Fig. 9 (corresponding values refer to Table S2, similarly hereinafter), high energy barriers up to about 0.8 eV exist in both OH(OH)23 and OH(OH)35 paths, indicating that the O-O bond in hydrogen peroxide is relatively stable. If the ionization happens around active sites of NCNTs, there is no energy barrier for the adsorption of H^+ and OOH^-. In details, H^+ is formed as hydronium to bond to the nitrogen atom and OOH^- bonds to the adjacent carbon atom, along with the electron transfer from anion to cation via nanotube. Comparing electronic structures of OOH(H)38 with OOH3 (See Figs. S10a and S5a), two peaks appear in the range of the high occupied energy level for OOH(H)38 and they are closer to Fermi level, suggesting that oxygen atoms become more activated due to the adsorption of proton. The highest occupied state of this system is a flat level, coinciding with Fermi level. The conductivity declines after proton adsorption.

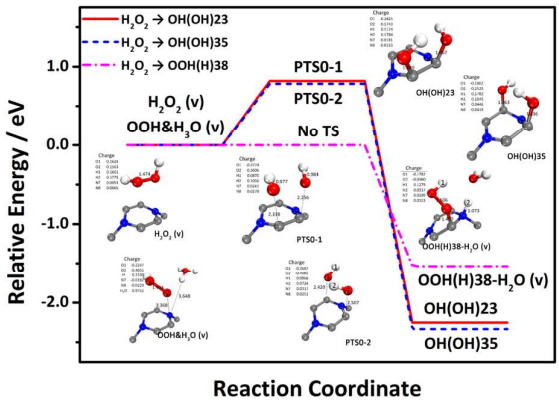

Fig. 9 Energy evolutions for the hydrogen peroxide molecule adsorption through cracked adsorption and ionized adsorption

For the first electron reaction in HPRR, only if one electron is imported from the outside to NCNTs and hydronium approaches to active sites, the reaction can proceed without dynamic energy barriers to generate O(H)38 or OH3 (See Fig. 10a). According to the analyses above, OH3 is more stable in

thermodynamics. In the view of structures, the C-N bond of O(H)38 is broken, so the carbon bonding to oxygen is under an active hybridization. In order to judge the mutual transformation of OH3 and O(H)38, PTS1-1 was searched out and the corresponding energy barrier is 0.672 eV, which is mainly applied for regeneration of the C-N bond and the migration of hydrogen. Nevertheless it is not an electrochemical process, the transformation rate is not very fast under such a barrier, meaning that the product O(H)38 can be remained at this step.

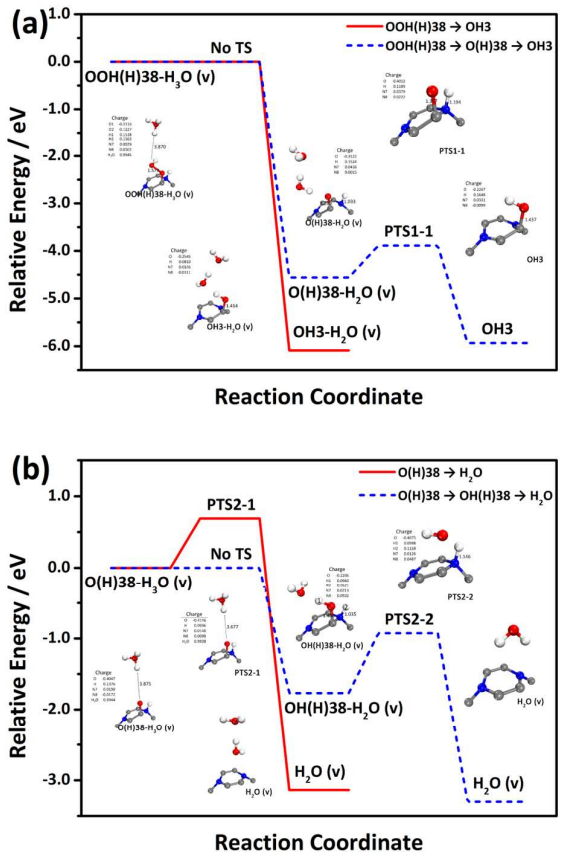

Fig. 10 Energy evolutions for (a) the first electron reaction in HPRR from the probable initial system OOH(H)38, and (b) the second electron reaction in HPRR from the probable initial system O(H)38.

For the second electron reaction in HPRR, it is same with the fourth electron reaction in ORR starting from OH3 (See Fig. 8). So we only consider the O(H)38 reactant in Fig. 10b. The red line represents an one-step reaction through the co-desorption of oxygen and hydrogen. The energy of 0.690 eV is needed to reach PTS2-1, with the negative charge enrichment at oxygen and regeneration of the C-N bond. The blue line represents a two-step reaction. First, hydronium can react with the oxygen atom easily in an electrochemical process, generating the intermediate OH(H)38. Then the hydroxyl is desorbed to combine with the adjacent hydrogen, which is controlled by the formation of PTS2-2. The whole process needs at least 0.843 eV. Comparing OH(H)38 with OH3, it is confirmed that the hydroxyl bonding to carbon is more favorable to react with the proton in solution rather than the adsorbed hydrogen. In conclusion, the reactant O(H)38 can transform to H_2O via one-step electroreduction with a low rate. The most transforms to OH(H)38 rapidly but it is difficult to continue generating H_2O, meaning that the intermediate OH(H)38 can remain in the system to be involved in other reactions.

The hydrogen peroxide disproportionation (HPD) should be considered to figure out the complicated transformation of intermediates in ORR and HPRR. We designed the two-step mechanism, as described by the following reaction Eqs. (8) and (9):

$$CNT + H_2O_2 + H^+ \rightarrow [CNT \cdots OH]^+ + H_2O \qquad (8)$$

$$[CNT \cdots OH]^+ + OOH^- \rightarrow H_2O + O_2 \qquad (9)$$

where H^+ comes from the acidic solution or the ionization of H_2O_2, and OOH^- only comes from the ionization of H_2O_2. The role of NCNTs catalyst is to transfer electrons between the hydrogen peroxide so as to accelerate the disproportionation. The details of transformation steps and the variations of energy are shown in Fig. 11. The hydrogen peroxide molecule, which is under the physisorption with active sites, obtains one electron from nanotubes and breaks the O-O bond to reach DTS1. Differing from the pure cracked adsorption, one of hydroxyls is combined with hydronium instead of bonding to carbon. For this step, the energy barrier is only 0.391 eV so it proceeds in a high rate. In the next step, OOH^- reacts with the intermediate OH3 and one electron transfers from anion to the positive charged nanotubes. The C-O bond is elongated and the hydroxyl is desorbed from nanotubes to reach DTS2, where the energy barrier is 0.434 eV. Along with the finally exergonic process, the hydrogen migrates from OOH to OH, finishing the disproportionation started from two hydrogen peroxide molecules. The rate determining step for the overall reaction is the desorption of hydroxyl in step 2.

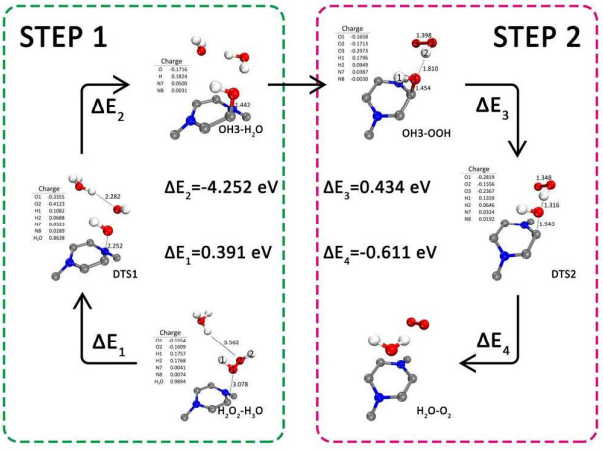

Fig. 11 The two-step disproportionation mechanism of hydrogen peroxide catalyzed by NCNTs in acidic electrolyte.

The mixed mechanism for ORR

According to the calculated energy variations for each process, the most reliable transformation path for the direct four-electron ORR is shown as Eq.(10). The rate determining step is the last process, whose energy barrier is 0.729 eV.

$$O_2 \rightarrow OO23 \rightarrow OOH3 \rightarrow O3 \rightarrow OH3 \rightarrow H_2O \qquad (10)$$

The most reliable transformation path for the two-electron ORR is shown as Eq.(11). The rate determining step is the last process, whose energy barrier is 0.313 eV.

$$O_2 \rightarrow OO23 \rightarrow OOH3 \rightarrow H_2O_2 \qquad (11)$$

The most reliable transformation path for the two-electron HPRR is shown as Eq.(12). The rate determining step is the last process, whose energy barrier is 0.690 eV.

$$H_2O_2 \rightarrow OOH(H)38 \rightarrow O(H)38 \rightarrow H_2O \qquad (12)$$

The most reliable transformation path for the hydrogen peroxide disproportionation is determined by step 2, whose energy barrier is 0.434 eV.

It is noteworthy that all the rate determining steps are related to the bonding hydroxyl because of the strong interaction between hydroxyl and carbon. Based on our calculations, the intermediate OH3 can participate in three reactions, including ORR, HPRR and HPD. Because of the difference of barriers, there is a competitive mechanism that OH3 is easy to be shifted into disproportionation while it is difficult to proceed in ORR and HPRR. Thence, we put forward the mixed mechanism as shown in Fig. 12. Due to the low energy barrier, O_2 can transform to H_2O_2 rapidly via a two-electron path (Blue line). A few hydrogen peroxide dissociate in the aqueous solution after the diffusion away from NCNTs (Orange line). Most of hydrogen peroxide molecules are involved in disproportionation with a high rate on the surface of NCNTs (Green line), instead of electroreduction. At the same time O_2 can obtain three electrons to generate the chemisorbed hydroxyl intermediate (Red line), which participates in the disproportionation. Under such a reaction cycle, the electron transfer number maintains from 2 to 4.

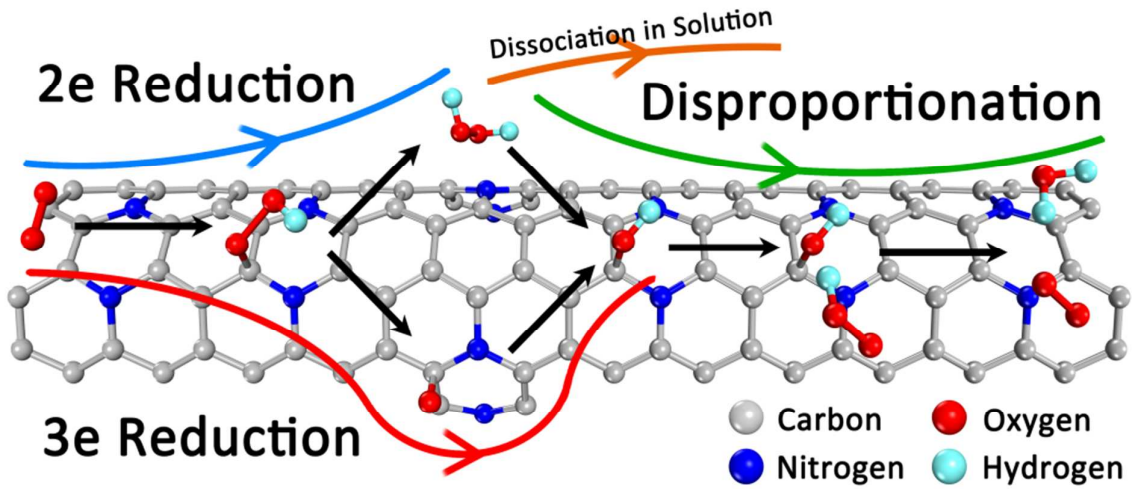

Fig. 12 Summarized transformation steps of oxygen in the overall acidic reduction reaction on NCNTs.

Analysis of experimental results

In order to illustrate the rationality of theory calculations, we studied experimentally oxygen reduction reaction catalyzed by NCNTs in acidic electrolyte. The NCNTs were synthesized by a chemical vapor deposition as previously reported[35]. The as-prepared NCNTs were treated with 6 M HCl for 2 h to remove the metal impurities. Electrochemical measurements were performed at room temperature in a three-electrode cell connected to an electrochemical analyzer (CH Instruments 760D) and a rotator (Pine Instrument Co.). The preparation of electrodes was described in our previous report[36]. The apparent electron transfer number (n) per oxygen molecule involved was calculated on the basis of the Koutecky-Levich (K-L) equation:

$$I^{-1} = I_K^{-1} + \left(0.62nFCD^{2/3}\nu^{-1/6}\omega^{1/2}\right)^{-1} \qquad (13)$$

where I is the measured current density, I_K is the kinetic current density of the ORR, n is the overall number of electron transferred during the oxygen reduction, F is the Faraday constant (F = 96485 C·mol^{-1}), C is the bulk concentration of O_2 (1.6×10^{-3} mol·L^{-1} in 1 M $HClO_4$), D is the diffusion coefficient of O_2 (1.1×10^{-5} cm^2·s^{-1} in 1 M $HClO_4$), ν (0.01 cm^2·s^{-1} in 1 M $HClO_4$) is the kinetic viscosity of the electrolyte, and ω is the angular velocity of the disk ($\omega = 2\pi N$, N is the linear rotation speed).

Linear sweep voltammograms (LSV) and the fitting result of the K-L equation at -0.25 V are shown in Fig. 13. The calculated apparent electron transfer number is 3.086, which can be explained by the mixed ORR mechanism. First, some oxygen molecules are reduced to hydrogen peroxide via the two-electron path and the other oxygen molecules are reduced to the intermediate hydroxyl via the three-electron path, where both processes are in a high rate. The generated H_2O_2 and OH

can both participate in the disproportionation rapidly, where two H_2O_2 molecules can regenerate one O_2 molecule. With such a reaction cycle, there is equivalently one half of oxygen going through the electroreduction, leading to the electron transfer number ranging from 2 to 4. Under the real condition, a part of generated H_2O_2 will dissociate slowly in the solution phase because of the diffusion away from the electrode surface. On the other hand, although the energy barrier of the direct four-electron ORR is relatively high, a small number of oxygen can also proceed along this path at the high electrode potential. Even under the low potential, this four-electron reduction may happen due to the electron tunneling effect[37], especially for nanoscale materials.

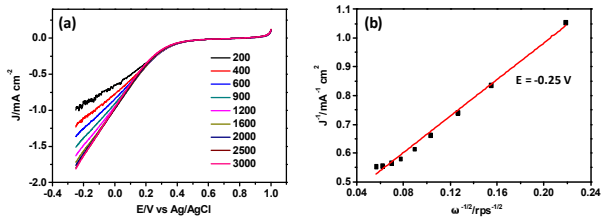

Fig. 13 (a) LSV and (b) K-L plots of NCNTs at different rotation rates in oxygen-saturated 1.0 M $HClO_4$ solution at a scan rate of 10 mV·s^{-1}.

Conclusions

ORR catalyzed by NCNTs in acidic electrolyte is an indefinable process. DFT calculations with the long range interaction correction and the COSMO modeling were performed to evaluate the hydronium migration process from bulk phase to graphitic NCNTs surface. The strong positive potential in the compact layer, which is caused by the polarization effect of charged NCNTs, is adverse to the hydronium approach. So the additional energy is needed to attract hydronium. The elementary transformations and energy variations of all the probable intermediates in ORR and HPRR were evaluated, where all the rate determining steps are related to the bonding hydroxyl because of the strong interaction between hydroxyl and carbon. Hence, the direct four-electron ORR and the two-electron HPRR are hard to proceed over graphitic NCNTs. Depending on the dynamic feasibility, a reliable mixed mechanism for ORR in acidic electrolyte was summarized in Fig. 12, where the two-electron, three-electron ORRs and HPD dominate the electrode reaction. Only a small percentage of oxygen goes through the direct four-electron reduction with a low rate, and few hydrogen peroxide enters the two-electron reduction. As a consequence, the apparent electron transfer number shows near 3, and hard to reach 4 at relative high potentials. The experimental result for ORR catalyzed by NCNTs in acidic electrolyte also well illustrated the rationality of theoretical calculations.

Acknowledgements

We acknowledge the financial support from the National Natural Science Foundation of China (No. 21373091, 21133010), the Guangdong Provincial Natural Science Foundation (No. S20120011275, 2014A030312007, 2013B090500023) and Program for New Century Excellent Talents in Universities of China (NCET-12-0190). We thank for the support by Information and Network Engineering and Research Center, SCUT.

Notes and references

1 H. A. Gasteiger, S. S. Kocha, B. Sompalli and F. T. Wagner, *Appl. Catal. B: Environ.*, 2005, **56**, 9.
2 M. Winter and R. J. Brodd, *Chem. Rev.*, 2004, **104**, 4245.
3 K. Gong, F. Du, Z. Xia, M. Durstock and L. Dai, *Science*, 2009, **323**, 760.
4 G. L. Tian, M. Q. Zhao, D. Yu, X. Y. Kong, J. Q. Huang, Q. Zhang and F. Wei, *Small*, 2014, **10**, 2251.
5 M. Yang, D. Yang, H. Chen, Y. Gao and H. Li, *J. Power Sources*, 2015, **279**, 28.
6 G. L. Chai, Z. Hou, D. J. Shu, T. Ikeda and K. Terakura, *J. Am. Chem. Soc.*, 2014, **136**, 13629.
7 S. Kundu, T. C. Nagaiah, W. Xia, Y. Wang, S. V. Dommele, J. H. Bitter, M. Santa, G. Grundmeier, M. Bron, W. Schuhmann and M. Muhler, *J. Phys. Chem. C*, 2009, **113**, 14302.
8 C. V. Rao, C. R. Cabrera and Y. Ishikawa, *J. Phys. Chem. Lett.*, 2010, **1**, 2622.
9 M. Li, L. Zhang, Q. Xu, J. Niu and Z. Xia, *J. Catal.*, 2014, **314**, 66.
10 L. Zhang and Z. Xia, *J. Phys. Chem. C*, 2011, **115**, 11170.
11 C. H. Choi, H. K. Lim, M. W. Chung, J. C. Park, H. Shin, H. Kim and S. I. Woo, *J. Am. Chem. Soc.*, 2014, **136**, 9070.
12 V. Neburchilov, J. Martin, H. Wang and J. Zhang, *J. Power Sources*, 2007, **169**, 221.
13 M. N. Huda and A. K. Ray, *Eur. Phys. J. B*, 2004, **40**, 337.
14 M. N. Huda and A. K. Ray, *Eur. Phys. J. B*, 2005, **43**, 131.
15 M. Terrones, P. M. Ajayan, F. Banhart, X. Blase, D. L. Carroll, J. C. Charlier, R. Czerw, B. Foley, N. Grobert, R. Kamalakaran, P. Kohler-Redlich, M. Rühle, T. Seeger and H. Terrones, *Appl. Phys. A: Mater. Sci. Process.*, 2002, **74**, 355.
16 S. Maldonado, S. Morin and K. J. Stevenson, *Carbon*, 2006, **44**, 1429.
17 M. Zhao, Y. Xia, J. P. Lewis and R. Zhang, *J. Appl. Phys.*, 2003, **94**, 2398.
18 N. Alexeyeva, E. Shulga, V. Kisand, I. Kink and K. Tammeveski, *J. Electroanal. Chem.*, 2010, **648**, 169.
19 Q. Shi, F. Peng, S. Liao, H. Wang, H. Yu, Z. Liu, B. Zhang and D. Su, *J. Mater. Chem. A*, 2013, **1**, 14853.
20 L. Carrette, K. A. Friedrich and U. Stimming, *ChemPhysChem*, 2000, **1**, 162.
21 B. Delley, *J. Chem. Phys.*, 2000, **113**, 7756.
22 J. P. Perdew, K. Burke and M. Ernzerhof, *Phys. Rev. Lett.*, 1996, **77**, 3865.
23 S. Grimme, *J. Comput. Chem.*, 2006, **27**, 1787.
24 A. Klamt and G. Schüürmann, *J. Chem. Soc., Perkin Trans. 2*, 1993, (5), 799.
25 B. Delley, *Mol. Simul.*, 2006, **32**, 117.
26 T. A. Halgren and W. N. Lipscomb, *Chem. Phys. Lett.*, 1977, **49**, 225.
27 G. Henkelman and H. Jónsson, *J. Chem. Phys.*, 2000, **113**, 9978.
28 F. L. Hirshfeld, *Theor. Chim. Acta*, 1977, **44**, 129.
29 L. I. Yeh, M. Okumura, J. D. Myers, J. M. Price and Y. T. Lee, *J. Chem. Phys.*, 1989, **91**, 7319.

30 M. Tuckerman, K. Laasonen, M. Sprik and M. Parrinello, *J. Chem. Phys.*, 1995, **103**, 150.
31 G. Tocci, L. Joly and A. Michaelides, *Nano Lett.*, 2014.
32 M. Kamiya, S. Saito and I. Ohmine, *J. Phys. Chem. B*, 2007, **111**, 2948.
33 S. Rastgar, H. Deng, F. Cortés-Salazar, M. D. Scanlon, M. Pribil, V. Amstutz, A. A. Karyakin, S. Shahrokhian and H. H. Girault, *ChemElectroChem*, 2014, **1**, 59.
34 F. Li, B. Su, F. C. Salazar, R. P. Nia and H. H. Girault, *Electrochem. Commun.*, 2009, **11**, 473.
35 Y. Cao, H. Yu, J. Tan, F. Peng, H. Wang, J. Li, W. Zheng and N.-B. Wong, *Carbon*, 2013, **57**, 433.
36 G. Zhong, H. Wang, H. Yu and F. Peng, *Fuel Cells*, 2013, **13**, 387.
37 E. Foxman, P. McEuen, U. Meirav, N. Wingreen, Y. Meir, P. Belk, N. Belk, M. Kastner and S. Wind, *Phys. Rev. B*, 1993, **47**, 10020.